Continuous Control Set Model Predictive Control of a Bridgeless-Boost Three-Level Active Rectifier

Vitor Monteiro
Centro ALGORITMI
University of Minho
Guimaraes, Portugal
vmonteiro@dei.uminho.pt

Jose A. Afonso
CMEMS
University of Minho
Guimaraes, Portugal
jose.afonso@dei.uminho.pt

Ana Rodrigues
Centro ALGORITMI
University of Minho
Guimaraes, Portugal
arodrigues@dei.uminho.pt

Tiago J. C. Sousa
Centro ALGORITMI
University of Minho
Guimaraes, Portugal
tsousa@dei.uminho.pt

Joao L. Afonso
Centro ALGORITMI
University of Minho
Guimaraes, Portugal
jla@dei.uminho.pt

***Abstract*—Over the past few decades, active rectifiers have assumed an important preponderance for numerous applications that propose to minimize power quality problems. Consequently, digital control algorithms are following this trend by contributing with a significant set of advantages. This paper presents the use of a continuous control set model predictive control (CCS-MPC) for a bridgeless-boost three-level (BB3L) active rectifier. The BB3L has a set of advantages when confronted with traditional solutions to improve power quality, where the possibility to operate with three voltage levels, sinusoidal current and unitary power factor, while using few switching devices, are the main features. Considering the multiplicity of applications for the BB3L active rectifier, the CCS-MPC is applied to obtain a robust current tracking. The BB3L is presented in detail throughout the paper and based on its mathematical model, the digital control equations are formulated, highlighting that the possibility of operating with a fixed switching frequency is the main characteristic. The results are achieved for many operating conditions, covering steady-state and transient-state, validating the accurate application of the CCS-MPC.**

***Keywords*—Continuous Control Set Model Predictive Control, Bridgeless-Boost Three-Level Active Rectifier, Power Quality.**

I. INTRODUCTION

The paradigm of smart grids is strongly influencing the appearance of new technologies to deal with environmental and sustainable matters, including technologies related to electric mobility, renewable energy resources, and power quality [1][2]. Regarding power quality, power-factor-correction converters, also identified as active rectifiers, are introduced as front-end converters for several applications in smart grids [3][4], permitting to reduce the total harmonic distortion (THD) of the grid-side current and the operation with high power factor [5][6]. Specifically, the boost-type structures are the most common for application as front-end converters in active rectifiers [7][8][9]. Despite the different existing structures of active rectifiers, specifically, this paper presents the continuous control set model predictive control (CCS-MPC) applied to a bridgeless-boost three-level (BB3L) active rectifier. The BB3L active rectifier was firstly proposed in [10], where it was exposed for applications in smart grids, whenever it is required to control the grid-side current. In terms of power electronics structure, the BB3L active rectifier is constituted by four passive power devices (diodes *d1*, *d2*, *d3*, and *d4*, forming a passive converter), and by two active power switches (*sa* and *sb*, forming a bipolar and bidirectional element, which can be controlled individually or as a single power switch), as shown in Fig. 1.

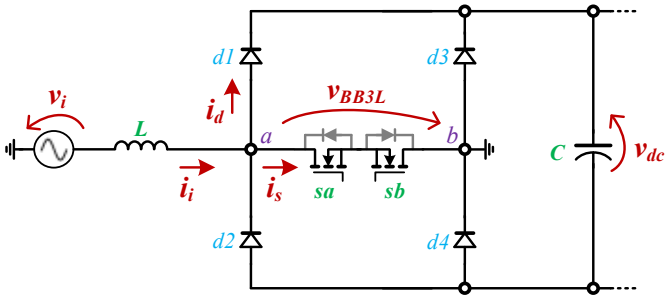

Fig. 1. Topology of the bridgeless-boost three-level (BB3L) active rectifier.

Nowadays, digital controllers are continually evolving, both in terms of costs and new built-in features to improve performance, being more attractive than analog controllers. Within digital controllers, hysteresis-band controllers and linear-controllers with pulse-width modulation (PWM) [11] are the most popular for wide applications and generally present satisfactory results (but can also present a set of drawbacks, e.g., variable switching frequency and resonance phenomena). Gradually, predictive controllers have gained more attention for a wide variety of applications [12][13][14][15][16]. Compared to conventional controllers, it is possible to consider the nonlinearities of the converter, as well as being more intuitive to understand and apply; nonetheless, as main handicap, presenting a more complex digital implementation. Numerous predictive controllers can be implemented, including the variants: finite control set (FCS) and continuous control set (CCS) [17][18][19][20]. When the objective is to control a grid-side current, as the case of the BB3L active rectifier, any controller can be applied, permitting to obtain good results in terms of following the reference. Nevertheless, when the control objective is to guarantee the operation with fixed switching frequency (e.g., with the objective of simplify the design of the passive filters and to minimize electromagnetic interferences), the CCS-MPC is the most convenient.

In the scope of this paper, a CCS-MPC is applied to the BB3L active rectifier, requiring a cost function and a modulator. The computation time needed depends on the considered prediction horizon. In each period, the state that diminishes the error is defined. Moreover, a longer prediction horizon (more than 1 [21]), can also be implemented to control the grid-side current of the BB3L active rectifier. As leading contributions of this paper, it can be emphasized: (a) CCS-MPC applied to the BB3L active rectifier, where the grid-side current is controlled with a fixed switching frequency; (b) Detailed explanation of the CCS-MPC; (c) Validation under steady-state and transient-state conditions regarding the reference current. A theoretical analysis of the BB3L active rectifier is presented in section II, where the details of its principle of operation are presented and used as support to a meticulous explanation of the CCS-MPC shown in section III. The validation is presented in section IV for the most interesting conditions of operation, permitting to support the feasibility of the CCS-MPC applied to control the grid-side current, as well as to establish a set of conclusions, given in section V.

II. Theoretical Analysis of the BB3L Active Rectifier

The topology of the BB3L active rectifier is presented in Fig. 1. As shown, it is constituted by four passive power devices (diodes *d1* to *d4*) and by two active power switches (MOSFETs in this case, *sa* and *sb*). As coupling filter with the power grid, an inductor (L) was considered to facilitate the understanding of the CCS-MPC controller and its digital implementation; however, obviously, other coupling filters can be considered, e.g., based on *LC* or *LCL*. Scrutinizing with detail the internal currents of the BB3L active rectifier, it is possible to identify that the grid-side current (i_i) is formed by the sum of the currents identified as i_d and i_s. From the point of view of the operating voltage levels, the current i_d is related to the operating levels v_{dc} and -v_{dc} and the current i_s is related to the operating level 0 (based on the topology, two distinct voltage levels can be defined). The operating voltage of the BB3L active rectifier (v_{BB3L}) is measured between the points *a* and *b*, according to the representation in Fig. 1.

When compared with the conventional power-factor-correction based on the boost dc-dc, the BB3L active rectifier requires one more switching device, but one less diode. However, the two switching devices are not controlled at the same time, i.e., one of them is controlled during the positive half-cycle and the other during the negative half-cycle. Moreover, in the BB3L active rectifier, the rms value of the circulating current in the main diodes (*d1* to *d4*) is reduced, permitting to improve the efficiency. Additionally, for obtaining the operating voltage level 0, only the MOSFETs *sa* and *sb* are used (one MOSFET and the reverse diode of the other MOSFET), in counterpart to the two diodes and a switching device used with the conventional power-factor-correction based on the boost dc-dc. On the other hand, for obtaining the operating voltage levels +v_{dc} and –v_{dc}, the BB3L active rectifier only uses two diodes, while the conventional power-factor-correction based on the boost dc-dc requires the use of three diodes (i.e., an additional diode is used to form the boost dc-dc). In addition, the BB3L active rectifier also has the added value of being able to continue operating even in the event of a failure of the control system, operating as a diode rectifier in this situation. The same situation is also possible for the power-factor-correction based on the boost dc-dc; however, an extra diode is always used, contributing to increase losses compared to the BB3L active rectifier. Summarizing, independently of the operating level (+v_{dc}, 0, and –v_{dc}), the BB3L active rectifier always requires a reduced number of power devices; however, an extensive evaluation among the two topologies is out of the scope of this paper, since its focus is on the applicability of the CCS-MPC. Nevertheless, this brief comparison is useful to demonstrate the applicability and benefits of the BB3L active rectifier in detriment of the conventional based on the boost dc-dc.

III. CCS-MPC Applied to the BB3L Active Rectifier

As presented above-mentioned, the objective of the BB3L active rectifier is to control the grid-side current (i_i) based on a reference (i_i*) to ensure a sinusoidal current. In the scope of this paper, the power theory used to achieve the reference current (i_i*) is not investigated, since the principal objective is only to introduce and describe the CCS-MPC applied to the BB3L active rectifier. As demonstrated in section II, the BB3L active rectifier operates with three voltage levels, i.e., 0 and +v_{dc} (positive half-cycle), and 0 and –v_{dc} (negative half-cycle). Examining Fig. 1 in terms of voltages and currents among the BB3L active rectifier and the power grid, the conforming dynamic system model is established by (the internal resistance of L can be ignored without introducing negative relevance for the provided analysis):

$$L\frac{di_i(t)}{dt} + v_{BB3L}(t) - v_i(t) = 0\,, \tag{1}$$

where L is the filter inductor, i_i is the grid-side current, v_i is the grid-side voltage, and v_{BB3L} is the operating voltage of the BB3L active rectifier. The voltage v_{BB3L} is as indicated in Fig. 1, and it is mathematically defined according to:

$$v_{BB3L}(t) = u\,v_{dc}(t)\,, \tag{2}$$

where u is defined by the state of the MOSTFETs (on or off), by the positive or negative half-cycle of the grid-side voltage (v_i), and by the value of the current error (i.e., e_{ii}, the difference between the measured current and its reference), according to:

$$u = \begin{cases} +1 & if \quad (v_i > 0)\,\&\&\,(e_{ii} > 0) \\ 0 & if \quad \big((v_i \geq 0)\&\&(e_{ii} > 0)\big)\,||\,\big((v_i < 0)\&\&(e_{ii} < 0)\big) \\ -1 & if \quad (v_i < 0)\,\&\&\,(e_{ii} < 0) \end{cases}. \tag{3}$$

As abovementioned, the CCS-MPC is an answer for the problem introduced by the FCS-MPC in terms of controllability with inconstant switching frequency. Discretizing (1) at a sampling time of T_s and applying the forward Euler approximation, which is defined by:

$$\frac{di_i(t)}{dt} \approx \frac{i_i[k+1] - i_i[k]}{T_s}\,, \tag{4}$$

the resultant discrete-time dynamic system model is:

$$\frac{L}{T_s}(i_i[k+1] - i_i[k]) + \frac{v_{BB3L}[k]}{v_{dc}[k]} - v_i[k] = 0\,. \tag{5}$$

Analyzing (5), it can be recognized that $i_i[k+1]$ is the current that the BB3L active rectifier must reach after a whole control period $[k, k+1]$, independently of the measured current at instant

[k]. Thus, this current must be predicted during the control period [k, k+1], based on the measured variables acquired in [k], i.e., at the beginning of the control period [k, k+1]. Taking into account these necessary assumptions, (1) must be rewritten in function of the current i_i[k+1], resulting in:

$$i_i[k+1] = \frac{T_s}{L}\left(v_i[k] + \frac{v_{BB3L}[k]}{v_{dc}[k]}\right) + i_i[k]\,. \tag{6}$$

The current defined in (6) is the current that the BB3L active rectifier must reach at the end of the control period [k, k+1] and must be equal to the established reference for the same control period. Summarizing, the current i_i[k+1] must be equal to the reference current i_i*[k+1]. However, at this point, it is recognized that it is necessary to know the reference current for the instant [k+1], but the reference current is established at the instant [k]. With the objective to accomplish with this goal, a prediction for [k+1] is established for the reference current, based on the actual [k] and previous measures [k-1] and [k-2], according to the three-order extrapolation method based on:

$$i_i^*[k+1] = 3\,(i_i^*[k] - i_i^*[k-1]) + i_i^*[k-2]\,. \tag{7}$$

After the detailed explanation regarding the predicted current for the instant [k] based on the dynamic system model, as well as about how to obtain the reference current for the instant [k+1], the last stage before the PWM consists in considering the cost function defined by:

$$g = \lambda\,|\,i_i^*[k+1] - i_i[k+1]\,|\,, \tag{8}$$

to minimize the error of the grid-side current. As shown in (1), it is considered the absolute value of the error and a weighting factor defined by λ, defined according to the parameters of the BB3L active rectifier and the defined requirements for controlling the grid-side current (e.g., it can be determined aiming to control the THD or to minimize the current ripple). Besides, other cost function can be used to minimize the error of the grid-side current, generating an upper correction of superior errors when related to minor ones, such as:

$$g = \lambda\,|\,i_i^*[k+1] - i_i[k+1]\,|^2. \tag{9}$$

The output of the cost function, i.e., the state of the BB3L active rectifier that minimizes the grid-side current error, is then compared with the carrier of the PWM to define the state of the MOSFETs during each control period. The ripple of the grid-side current is defined in function of the grid-side voltage, the operating voltage, the duty-cycle (and sampling period), and the coupling filter, according to:

$$\Delta i_i = t_{on}\frac{v_i - v_{BB3L}}{LT_s}\,. \tag{10}$$

With the objective to assess the performance of the CCS-MPC, the percentage value of the error, can be verified by:

$$\%e_{ii} = \frac{\frac{1}{n}\sum_{k=0}^{n}|e_{ii}[k]|}{I_I}\,, \tag{11}$$

which corresponds to the absolute difference between the measured current and its reference, based on the number of samples, with respect to the rms value of the grid-side current.

To complement the analysis of the CCS-MPC applied to the BB3L active rectifier, the following points should be clarified: (i) In the control algorithm, the considered sampling frequency, for each input signal, corresponds to twice the switching frequency; The PWM carrier is of the center-aligned type; (ii) The comparison signal with the carrier is updated twice in each period of the carrier [k, k+2] (i.e., whenever the signals are sampled and the control algorithms are performed). As mentioned, the variables are acquired at the instant [k] and they remain with the same value throughout the period [k, k+1]. During this period [k, k+1], according to the considered PWM carrier, the current takes on three distinct stages: negative slope, positive slope and, again, negative slope (depending on the half-cycle, positive or negative, the stages can do otherwise, i.e., positive slope, negative slope and, again, positive slope). Based on the system dynamics equation, the current i_i for the instant [k+1] can be determined as a function of the other variables (i.e., i_i, v_i and v_{BB3L} for the instant [k]). The current i_i is sampled at time [k] and the current at time [k+1] is the desired at the end of a control cycle [k, k+1]. To cancel the error at the end of a control cycle, the current at time [k+1] must be equal to its reference, also at time [k+1]. For this, the extrapolation equation is used to obtain i_i*[k+1]. Obviously, this process is cyclical, being repeated twice in each period of the PWM carrier. In other words, during a period of the PWM carrier (i.e., [k, k+2]) the current sampled in [k] reaches its reference in [k+1] and, subsequently, the current sampled in [k+1] reaches its reference in [k+2].

IV. Analysis and Validation of the CCS-MPC Applied to the BB3L Active Rectifier

The validation of the CCS-MPC applied to the BB3L active rectifier was conducted with a developed model in PSIM and according to the conditions listed in Table I. As mentioned, it is not an objective of this paper to deal with any specific power theory, and the rms value and waveform of the reference current was determined according to the operating power.

TABLE I
Characteristics of the BB3L Active Rectifier

Parameter	Value
Rms value of the Grid-Side Voltage	230 V
Switching Frequency	100 kHz
Sampling Frequency	200 kHz
Nominal dc-link Voltage	400 V
Maximum Operating Power	3.5 kW
Coupling Inductor Filter	500 µH
Output Resistive Load	46 Ω

Based on the simulation results, Fig. 2 shows the current i_i and its reference (i_i*) for two sampling periods [k, k+1] and [k+1, k+2], which correspond to a PWM carrier period of [k, k+2]. This result was obtained for the positive half-cycle. As it can be seen, in this specific case, in the period [k, k+1] the current i_i has two distinct stages: initially with a negative slope and, later, with a positive slope. In the period [k+1, k+2], there are also two distinct stages, but in a different sequence: initially with a positive slope and, later, with a negative slope. As it can be seen, at the end of each sampling period, the current i_i reaches its reference i_i*, thus fulfilling the main objective of the CCS-MPC. Also, in Fig. 2 is shown the PWM carrier (c_{PWM}),

and the comparison signal (a_{pwm} and b_{pwm}) with the PWM carrier to obtain the control for the MOSFETs *sa* and *sb*, respectively. As this result refers to the negative half-cycle, it is controlled the MOSFET *sa*, while the MOSFET *sb* is always off. As it can be seen, both the reference current (i_i*) and the comparison signals (a_{pwm} and b_{pwm}) with the carrier (c_{PWM}) are determined at each instant [*k*].

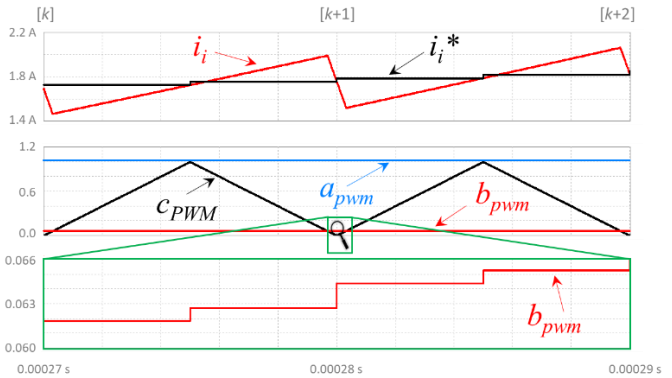

Fig. 2. Principle of operation of the CCS-MPC applied to the BB3L active rectifier during the positive half-cycle: Grid-side current (i_i); Grid-side reference current (i_i*); PWM carrier (c_{PWM}); Control signals (a_{pwm}, b_{pwm}).

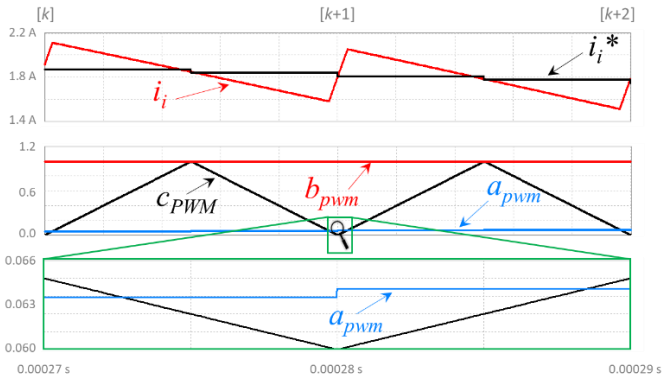

Fig. 3. Principle of operation of the CCS-MPC applied to the BB3L active rectifier during the negative half-cycle: Grid-side current (i_i); Grid-side reference current (i_i*); PWM carrier (c_{PWM}); Control signals (a_{pwm}, b_{pwm}).

Similarly, the same occurs in the negative half-cycle, as it can be seen in Fig. 3. In this case, in the period [*k*, *k*+1], initially, the current presents a positive slope and, later, a negative slope. In the period [*k*+1, *k*+2] occurs precisely the opposite. As this result refers to the negative half-cycle, it is controlled the MOSFET *sb*, while the MOSFET *sa* is always off. In Fig. 4 are shown the current i_i, the PWM carrier (c_{PWM}), and the comparison signals with the carrier (a_{pwm} and b_{pwm}) to obtain the control signals of each MOSFET, during a cycle of the grid-side voltage. As it can be seen, the current i_i is perfectly sinusoidal and, in each half-cycle, only one of the MOSFETs is controlled.

Fig. 5 shows the grid-side voltage (v_i), the grid-side current (i_i), and the operating voltage of the BB3L active rectifier (v_{BB3L}). These results were obtained considering two different situations of the power grid: a sinusoidal voltage waveform and a voltage with harmonic content (THD of 3.6%). In both situations, the current i_i is sinusoidal and it is in phase with the voltage. In addition, as it can be seen, the operating voltage v_{BB3L} has always three different levels (+v_{dc}, 0, and -v_{dc}). The current i_i is always sinusoidal, because a phase-locked loop (PLL) algorithm is used to obtain a reference current solely dependent on the fundamental component of the grid-side voltage.

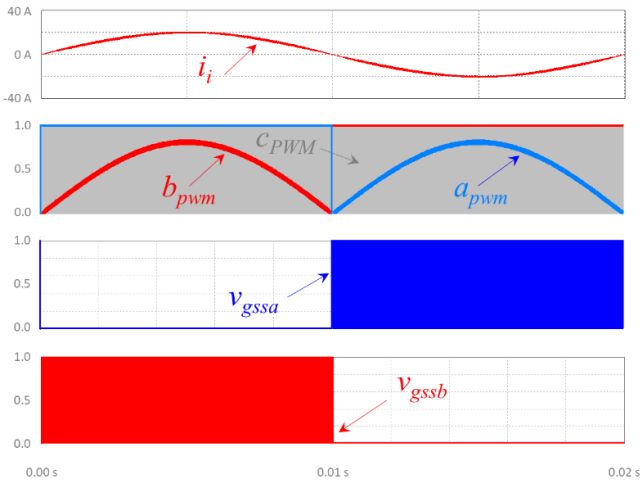

Fig. 4. Principle of operation of the CCS-MPC applied to the BB3L active rectifier during a complete period of the grid-side voltage: Grid-side current (i_i); PWM carrier (c_{PWM}), Control signals (a_{pwm}, b_{pwm}); Gate-source voltage of the MOSFETs *sa* and *sb* (v_{gssa}, v_{gssb}).

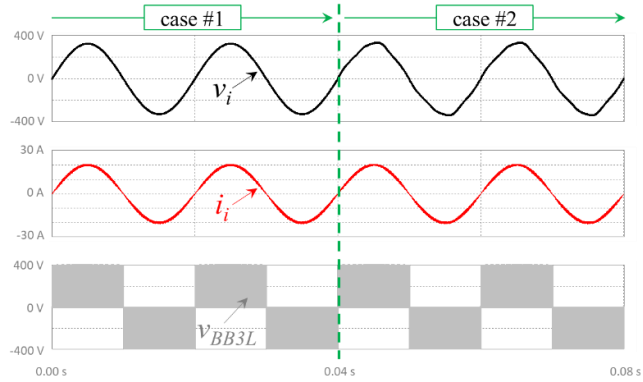

Fig. 5. BB3L active rectifier operating with a sinusoidal grid-side current: Grid-side voltage (v_i); Grid-side current (i_i); Operating voltage (v_{BB3L}).

In Fig. 6 it is shown a detail of the same variables to visualize the division of the currents internally in the BB3L active rectifier. As it can be seen, in this specific detail, the current i_i is constituted by the currents in the diode *d1* and in the MOSFET *sb*. The evolution of the current i_i is shown in Fig. 7 when there is a sudden change in the reference current (i_i*). In this specific case, a 25% increase in the reference current (i_i*) was considered. As it can be seen, despite the sudden variation, the current i_i follows its reference, i.e., it reaches the steady-state again in just two control cycles, representing an important characteristic of the CCS-MPC. This figure also shows the PWM carrier and the respective comparison signal, as well as the gate-source voltage applied to control the MOSFET *sb*. In addition to 1 prediction horizon, other horizons can be considered. For example, by forcing to extrapolate the reference current to [*k*+2] using equation (7), it is possible that the current i_i also follows its reference (i_i*), as shown in Fig. 8. However, when sudden changes occur, the current i_i takes more control cycles before reaching the steady-state again. One of these examples is shown in Fig. 8, where a 25% increase in the

reference current was considered (as in the previous situation), but in this case, as when the horizon assumes the value 2, the current takes more control cycles to reach the steady-state.

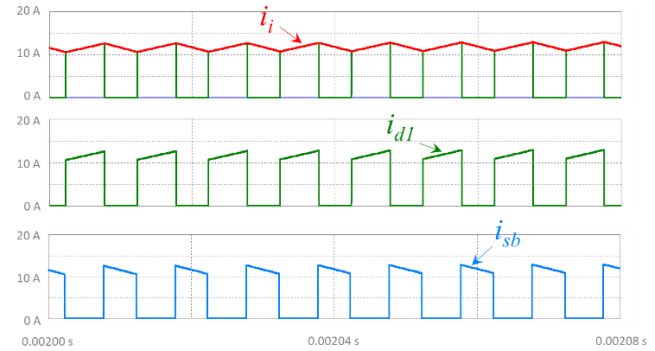

Fig. 6. Detail of the internal current division of the BB3L active rectifier: Grid-side current (i_i); Current in the diode *d1* (i_{d1}); Current in the MOSFET *sb* (i_{sb}).

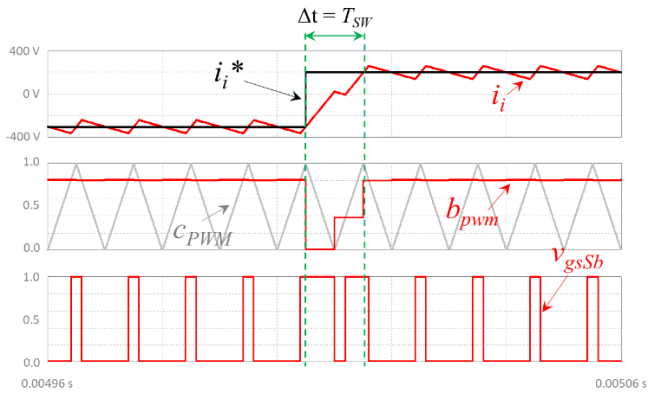

Fig. 7. Detail of the BB3L active rectifier operating in transient-state with 1 prediction horizon: Grid-side current (i_i); Grid-side reference current (i_i*); PWM carrier (c_{PWM}); Control signal (b_{pwm}); Gate-source voltage applied to the MOSFET *sb* (v_{gssb}).

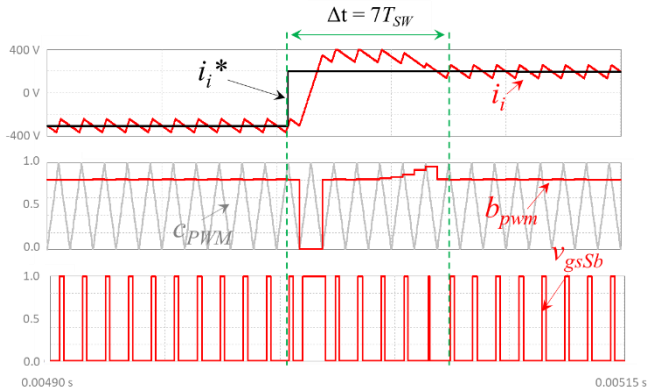

Fig. 8. Detail of the BB3L active rectifier operating in transient-state with 2 horizon prediction: Grid-side current (i_i); Grid-side reference current (i_i*); PWM carrier (c_{PWM}); Control signal (b_{pwm}); Gate-source voltage applied to the MOSFET *sb* (v_{gssb}).

Fig. 9 shows the current i_i and its reference i_i*, the PWM carrier (c_{PWM}) and the comparison control signals (a_{pwm} and b_{pwm}), as well as a detail of b_{pwm}, when considering a prediction horizon of 2. This result was obtained for two sampling periods [k, k+1] and [k+1, k+2], which corresponds to a PWM carrier period of [k, k+2]. As it can be seen, in the period [k, k+1] the current i_i has three distinct stages: initially with a negative slope, then with a positive slope, and, later, again with a negative slope. In the period [k+1, k+2], naturally, there are also three distinct stages with the same sequence. As it can be seen, at the end of each sampling period, the current i_i reaches its reference i_i*, thus fulfilling the main objective of the CCS-MPC controller applied to the BB3L active rectifier. As this result refers to the positive half-cycle, it is controlled the MOSFET *sb*, while the MOSFET *sa* is always off. As it can be seen, both the reference current (i_i*) and the comparison signals (a_{pwm} and b_{pwm}) with the carrier (c_{PWM}) are determined at each instant [k].

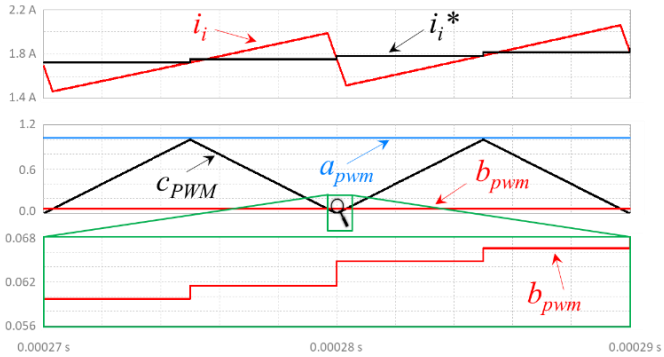

Fig. 9. Principle of operation of the CCS-MPC applied to the BB3L active rectifier during the positive half-cycle and with a 2 prediction horizon: Grid-side current (i_i); Grid-side reference current (i_i*); PWM carrier (c_{PWM}), Control signals (a_{pwm}, b_{pwm}).

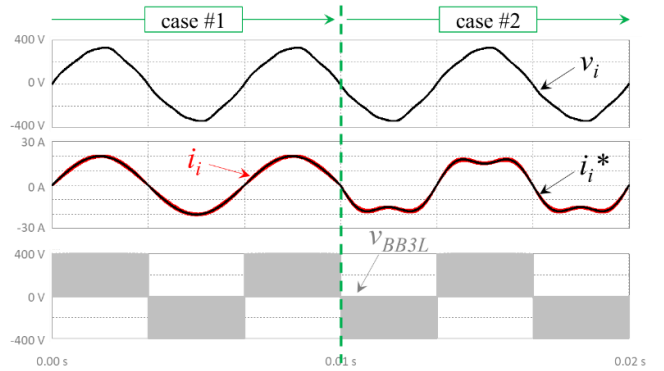

Fig. 10. BB3L active rectifier operating with a grid-side current containing a third harmonic in phase with the fundamental frequency of the grid-side voltage: Grid-side voltage (v_i); Grid-side current (i_i); Operating voltage (v_{BB3L}).

Fig. 10 shows a result that allows to validate the CCS-MPC applied to the BB3L active rectifier when the grid-side current is non-sinusoidal. This result is divided into two distinct cases. In case #1, the reference current is sinusoidal and, as it can be seen, the current i_i is also sinusoidal, in addition, the operating voltage of the converter has three voltage levels. In case #2, instead of a sinusoidal reference current, a reference with harmonic distortion was considered, specifically a current with a fundamental frequency of 150 Hz, an amplitude of 5 A, and the same phase as the grid-side voltage. The BB3L active rectifier allows to operate with the current i_i distorted, perfectly following its reference (i_i*). These values are merely indicative to validate the control, and other values, either of frequency or amplitude, can be used.

V. CONCLUSIONS

The importance of active rectifiers and digital control systems has been demonstrated for many applications targeting to improve power quality indices. By combining these two perspectives, this paper presents a continuous control set model predictive control (CCS-MPC) applied to a bridgeless-boost three-level (BB3L) active rectifier. The main features of the BB3L active rectifier were presented along the paper supported by a comparison with conventional solutions. Regarding the CCS-MPC, its mathematical deduction and the necessary details for the digital implementation are meticulously presented, where the operation with a fixed switching frequency is the core distinguishing attribute. The validation was performed for the main operating circumstances, showing that the grid-side current tracks its reference within a specified sampling period, considering real conditions of the grid-side voltage and distinct reference currents, including sinusoidal and non-sinusoidal, as well as with operating power in steady-state and in transient-state. Additionally, the application of 1 and 2 predictive horizons were considered and verified. Succinctly, this paper validated the applicability of the CCS-MPC to control a BB3L active rectifier with fixed switching frequency.

ACKNOWLEDGMENT

This work has been supported by FCT – Fundação para a Ciência e Tecnologia within the R&D Units Project Scope: UIDB/00319/2020. This work has been supported by the FCT Project newERA4GRIDs PTDC/EEI-EEE/30283/2017. Tiago J. C. Sousa is supported by the doctoral scholarship SFRH/BD/134353/2017 granted by FCT.

REFERENCES

[1] Vitor Monteiro, Bruno Exposto, Joao C. Ferreira, Joao L. Afonso, "Improved Vehicle-to-Home (iV2H) Operation Mode: Experimental Analysis of the Electric Vehicle as Off-Line UPS," IEEE Trans. Smart Grid, vol.8, no.6, pp.2702-2711, Nov. 2017.

[2] Shuang Gao, K. T. Chau, Chunhua Liu, Diyun Wu, C. C. Chan, "Integrated Energy Management of Plug-in Electric Vehicles in Power Grid with Renewables," IEEE Trans. Veh. Technol., vol.63, no.7, pp.3019-3027, Sept. 2014.

[3] Wenlong Qi, Sinan Li, Huawei Yuan, Siew-Chong Tan, Shu-Yuen Hui, "High-Power-Density Single-Phase Three-Level Flying-Capacitor Buck PFC Rectifier," IEEE Trans. Power Electron., vol.34, no.11, pp.10833-10844, Nov. 2019.

[4] Joseph Benzaquen, F. Fateh, M. B. Shadmand, Behrooz Mirafzal, "Performance Comparison of Active Rectifier Control Schemes in More Electric Aircraft Applications," IEEE Trans. Transportation Electrification, vol.5, no.4, pp.1470-1479, Dec. 2019.

[5] Bhim Singh, Brij N. Singh, Ambrish Chandra, Kamal Al-Haddad, Ashish Pandey, Dwarka P. Kothari, "A Review of Single-Phase Improved Power Quality AC-DC Converters," IEEE Trans. Ind. Electron., vol.50, no.5, pp.962-981, Oct. 2003.

[6] Vítor Monteiro, Bruno Exposto, J. G. Pinto, M. J. Sepúlveda, Andrés A. Nogueiras Meléndez, João L. Afonso, "Three-Phase Three-Level Current-Source Converter for EVs Fast Battery Charging Systems," IEEE ICIT International Conference on Industrial Technology, Seville Spain, pp.1401-1406, March 2015.

[7] André De Bastiani Lange, Thiago Batista Soeiro, Márcio Silveira Ortmann, Marcelo Lobo Heldwein, "Three-Level Single-Phase Bridgeless PFC Rectifiers," IEEE Trans. Power Electron., vol.30, no.6, pp.2935-2949, June 2015.

[8] Fariborz Musavi, Murray Edington, Wilson Eberle, William G. Dunford, "Evaluation and Efficiency Comparison of Front End AC-DC Plug-in Hybrid Charger Topologies," IEEE Trans. Smart Grid, vol.3, no.1, pp.413-421, Mar. 2012.

[9] Vitor Monteiro, Andres A. Nogueiras Melendez, Joao C. Ferreira, Carlos Couto, Joao L. Afonso, "Experimental Validation of a Proposed Single-Phase Five-Level Active Rectifier Operating with Model Predictive Current Control," IEEE IECON Industrial Electronics Conference, pp.3939-3944, Nov. 2015.

[10] Vitor Monteiro, Andres A. Nogueiras Melendez, Carlos Couto, Joao L. Afonso, "Model Predictive Current Control of a Proposed Single-Switch Three-Level Active Rectifier Applied to EV Battery Chargers," IEEE IECON Industrial Electronics Conference, Florence Italy, pp.1365-1370, Oct. 2016.

[11] M. Kazmierkowski, Luigi Malesani, "Current Control Techniques for Three-Phase Voltage-Source PWM Converters: A Survey," IEEE Trans. Ind. Electron., vol.45, no.5, pp.691-703, Oct. 1998.

[12] A. Dahlmann, Venkata Yaramasu, A. Dekka, Samir Kouro, S. Padmanaban, "Predictive Control of Two-Stage Grid-Connected Photovoltaic Energy System with Constant Switching Frequency," IEEE PEDG International Symposium on Power Electronics for Distributed Generation Systems, Croatia, pp.346-351, 2020.

[13] S. Liu, C. Liu, Y. Huang, H. Zhao, "Model Predictive Two-Target Current Control for OW-PMSM," IEEE Trans. Power Electron., vol.36, no.3, pp.3224-3235, Mar. 2021.

[14] Mostafa Abarzadeh, Nathan Weise, Ramin Katebi, Alireza Javadi, Kamal Al-Haddad, "Constant Switching Frequency Hierarchical Deadbeat Predictive Direct Power Controller with Dynamic Power Estimator for 3L-ANPC AFE Rectifier for EV Charger Applications," IEEE IETC Transportation Electrification Conference & Expo, Chicago USA, pp.1006-1011, 2020.

[15] P. Karamanakos, M. Nahalparvari, T. Geyer, "Fixed Switching Frequency Direct Model Predictive Control With Continuous and Discontinuous Modulation for Grid-Tied Converters With LCL Filters," IEEE Trans. Control Sys. Tech., pp.1-16, 2020.

[16] Su Zhang, Udaya Kumara Madawala, "A Hybrid Model Predictive Multilayer Control Strategy for Modular Multilevel Converters," IEEE Journal of Emerging and Selected Topics in Power Electronics, vol.7, no.2, pp.1002-1014, June 2019.

[17] M. -G. Farajzadeh-Devin, S. K. H. Sani, "Enhanced two-loop model predictive control design for linear uncertain systems," Journal of Systems Engineering and Electronics, vol.32, no.1, pp.220-227, Feb. 2021.

[18] J. Rodríguez, R. Heydari, Z. Rafiee, H. A. Young, F. Flores-Bahamonde, M. Shahparasti, "Model-Free Predictive Current Control of a Voltage Source Inverter," IEEE Access, vol.8, pp.211104-211114, 2020.

[19] Venkata Yaramasu, Marco Rivera, Bin Wu, J. Rodriguez, "Model Predictive Current Control of Two-Level Four-Leg Inverters—Part I: Concept, Algorithm, and Simulation Analysis," IEEE Trans. Power Electron., vol.28, no.7, pp.3459-3468, July 2013.

[20] Marco Rivera, Venkata Yaramasu, J. Rodriguez, Bin Wu, "Model Predictive Current Control of Two-Level Four-Leg Inverters—Part II: Experimental Implementation and Validation," IEEE Trans. Power Electron., vol.28, no.7, pp.3469-3478, July 2013.

[21] Patricio Cortes, Jose Rodriguez, Cesar Silva, Alexis Flores, "Delay Compensation in Model Predictive Current Control of a Three-Phase Inverter," IEEE Trans. Ind. Electron., vol.59, no.2, pp.1323-1325, Feb. 2012.